Gap solitons in Bose-Einstein condensate under moiré optical lattice*

TU Pu[1, 2], ZHAO Xi[1], XI Baolong[1], SHAO Kaihua[1], XI Zhonghong[1, 3], GOU Jinming[1], WANG Yongzhi[1], SHI Yuren[1, *]

1. College of Physics and Electronic Engineering, Northwest Normal University, Lanzhou 730070, China
2. College of Intelligent Manufacturing, Sichuan University of Arts and Science, Dazhou 635000, China
3. College of Energy and Power Engineering, Gansu Minzu Normal University, Hezuo 747000, China

Abstract

In this study, we investigate gap solitons and their stability in Bose-Einstein condensates confined in moiré optical lattices with different twist angles. The results demonstrate that the twist angle significantly modulates the moiré periodicity and the flatness of low bands. For sufficiently large angular differences, smaller twist angles generally lead to larger moiré periods and flatter low bands, although this trend becomes less consistent at the smallest angular differences. Moreover, smaller twist angles generate more complex potential structures. These structures modify the gap positions and widths, consequently affecting the properties of gap solitons. Using the Newton-conjugate gradient method, we identify various types of solitons in moiré lattice with four different twist angles, and observe that solitons can exist over a broader range of potential depths at smaller twist angles. The density distributions of solitons exhibit markedly different behaviors in different gaps: in the semi-infinite gap dominated by attractive interactions, deeper potentials lead to reduced soliton density, whereas in the first gap governed by repulsive interactions, deeper potentials enhance soliton density distributions. Linear stability analysis and nonlinear dynamical evolution results indicate that the solitons found in the first gap (including both

* The paper is an English translated version of the original Chinese paper published in Acta Physica Sinica. Please cite the paper as: TU Pu[1, 2], ZHAO Xi[1], XI Baolong[1], SHAO Kaihua[1], XI Zhonghong[1, 3], GOU Jinming[1], WANG Yongzhi[1], SHI Yuren[1, *], **Gap solitons in Bose-Einstein condensate under moiré optical lattice**. *Acta Phys. Sin.*, 2026, 75(3):030601.
doi: 10.7498/aps.75.20251307

single-humped and multi-humped structures) exhibit robust dynamical stability, that the single-humped solitons found in the semi-infinite gap maintain good stability, while closely separated multi-humped in-phase solitons tend to be unstable, and that enhanced stability is observed for solitons located closer to the band edges. This work provides a theoretical foundation for manipulating nonlinear solitons in moiré superlattices.

Keywords：moiré lattice; Bose-Einstein condensate; gap soliton; twist angle;

PACS：03.75.Lm; 05.30.Jp; 02.70.-c

DOI：10.7498/aps.75.20251307

CSTR: 32037.14.aps.75.20251307

1 Introduction

The interplay between spatial periodicity and nonlinear dynamical evolution can induce numerous intriguing many-body physical effects. One such phenomenon involves the excitation of localized nonlinear waves within the bandgaps of Bloch linear energy bands, known as gap solitons[1-5]. Gap solitons represent a novel type of localized mode in periodic physical systems, with their chemical potential situated within the bandgap of the linear energy spectrum. The localization properties of gap solitons offer potential applications in optical communication, optical control, and optical storage[6-10]. Previous studies have demonstrated that gap solitons can exist in various nonlinear periodic structures, with optical lattices serving as the most classic example[11-13]. Recently, a scheme using two overlapping optical lattices to simulate twisted bilayer optical lattices has garnered significant interest in the physics community. This structure is referred to as a moiré lattice[14-16]. The concept of moiré lattice structures originally emerged from twisted bilayer graphene, which exhibits a rich phase diagram when overlapped at a small relative angle[17-22]. The periodicity of a moiré lattice depends on the geometric parameters of the constituent lattices and their superposition method. Consequently, it may exhibit strict periodicity or form aperiodic structures. Taking a bilayer square lattice as an example, when two lattices are superimposed with a specific twist angle θ, the system forms a periodic Moiré superlattice if the angle satisfies commensurability conditions. Specifically, the rotated lattice vectors must be expressible as rational linear combinations of the original lattice vectors. When θ meets the Pythagorean angle condition, the translational symmetry of the moiré lattice is strictly preserved. In this case, the superlattice period is determined jointly by the original lattice constant and the twist angle, manifesting as a long-range ordered

periodic structure[14,16,23-26]. This characteristic makes moiré lattices an ideal platform for investigating localized excitation modes in periodic systems.

Ultracold atomic systems serve as a novel quantum simulation platform. Their clean environment and high tunability provide particularly advantageous conditions for soliton-related research. These systems not only advance frontier explorations in nonlinear physics, quantum many-body systems, and condensed matter physics but also offer potential new functional units for quantum technologies. Currently, many researchers are investigating solitons in Bose-Einstein condensates (BECs) within optical lattices[27-34]. However, most studies have focused on single-layer optical lattices, while research on gap solitons in BECs within bilayer optical lattices remains scarce[35-37]. In 2023, the research group led by Jing Zhang[38] successfully loaded a ^{87}Rb atomic BEC into a twisted bilayer optical lattice. This highly controllable external potential opens new directions for exploring Moiré physics in ultracold atoms. Existing studies indicate that multiple peaks appear when atoms are loaded into twisted bilayer optical lattices, supporting the confinement of atoms with different spin states in distinct lattices. The bandgap of a twisted bilayer square optical lattice is significantly larger than that of a single-layer square optical lattice[39]. Furthermore, band flattening phenomena similar to those in magic-angle graphene occur at specific angles[40-43]. Novel band structures in lattice systems often lead to new material functionalities and discoveries. In this novel system of BECs loaded into such optical lattices, it is worth investigating whether various control methods affect gap solitons similarly to single-layer lattice systems. It is also crucial to determine whether new quantum many-body effects arise. However, relevant research in this area remains limited. Our group has previously discussed in depth the effects of short-range contact interactions[44] and spin-orbit coupling[45] on gap solitons in moiré lattices. Nevertheless, the specific influences of the periodicity and lattice structure of the moiré lattice itself on solitons warrant further exploration.

We first investigate the periodic moiré lattice potentials and their corresponding linear band structures under different twist angles. The results indicate that the twist angle significantly affects the Moiré period length and lattice structure. For moiré lattices formed by the twisted superposition of square lattices, a smaller twist angle generally corresponds to a larger Moiré period and flatter low-energy bands when the angular difference is substantial. However, this rule does not fully hold when the angular difference is small. Subsequently, we employ the Newton-conjugate gradient method to identify various types of solitons within the semi-infinite bandgap and the first bandgap. We then investigate the dynamical stability of these solitons through linear stability analysis and long-time dynamical evolution simulations.

2 Theoretical Model

We consider a single-component BEC trapped in a moiré lattice formed by the twisted superposition of two square lattices. Within the mean-field approximation, the dynamical properties of the system are described by the following Gross-Pitaevskii equation (GPE)[45,46]:

$$\mathrm{i}\hbar\frac{\partial\Psi}{\partial t}=-\frac{\hbar^2}{2m}\nabla^2\Psi+V_{\mathrm{ext}}\Psi+g|\Psi|^2\Psi, \tag{1}$$

Here, $\Psi=\Psi(\boldsymbol{r},t)$ denotes the wave function, m represents the atomic mass, V_{ext} indicates the external potential, and $g=4\pi\hbar^2a_{\mathrm{s}}/m$ defines the strength of short-range contact interactions between atoms, where a_{s} is the s-wave scattering length. The total particle number of the system is given by $N=\int|\Psi|^2\mathrm{d}\boldsymbol{r}$. We assume that the system is strongly confined in the z direction by a harmonic oscillator potential with frequency ω_z, characterized by the length scale $a_z=\sqrt{\frac{\hbar}{m\omega_z}}$. Under these conditions, the three-dimensional Gross-Pitaevskii equation (GPE) reduces to a two-dimensional GPE via the quasi-two-dimensional approximation. We introduce the dimensionless variables $\tilde{t}=\omega_0t$, $\tilde{x}=x/a_0$, $\tilde{y}=y/a_0$, $\tilde{V}_{\mathrm{ext}}=V_{\mathrm{ext}}/\hbar\omega_0$, $\tilde{\Psi}=\Psi/\sqrt{{n_0}/{a_0}^2}$, and $\tilde{g}=2\sqrt{2\pi}n_0a_{\mathrm{s}}/a_z$. Here, $a_0=\sqrt{\hbar/m\omega_0}$, $\omega_0=\min\{\omega_x,\omega_y\}$, and n_0 is the specified particle number density, satisfying $N=n_0\int|\tilde{\Psi}|^2\mathrm{d}\tilde{x}\mathrm{d}\tilde{y}$. By omitting the tilde symbols over the variables, we obtain the following quasi-two-dimensional dimensionless GPE:

$$\mathrm{i}\frac{\partial\Psi}{\partial t}=-\frac{1}{2}\nabla^2\Psi+V_{\mathrm{ext}}\Psi+g|\Psi|^2\Psi. \tag{2}$$

In the experiment, one can select ^{87}Rb atoms to realize this BEC system. Under strong confinement by a harmonic potential well along the z direction with frequency $\omega_z=2\pi\times100$ Hz, a scattering length of $a_{\mathrm{s}}\approx40.6a_{\mathrm{B}}\approx2.15\mathrm{nm}$, and an atom number of $N=10^3$, the dimensionless contact interaction is $g\approx1$ [47,48]. Alternatively, ^{7}Li atoms may be chosen. When the confinement frequency along the z direction is $\omega_z=2\pi\times52$ Hz, the scattering length is $a_{\mathrm{s}}\approx-10a_{\mathrm{B}}\approx-0.529\mathrm{nm}$, and the atom number is $N=10^3$, the dimensionless contact interaction becomes $\mathrm{g}\approx-0.5$[49].

The external potential consists of the superposition of two square optical lattices, $V_1(x,y)$ and $V_2(x',y')$, rotated by an angle θ relative to each other. Its expression is given as[38,45]

$$V_{\text{ext}}(x,y) = \begin{array}{l} p_1[\cos(kx)+\cos(ky)] \\ +p_2[\cos(kx')+\cos(ky')], \end{array} \quad (3)$$

Here, p_1 and p_2 denote the amplitudes of sublattices V_1 and V_2, respectively, while k represents the lattice constant. The coordinates (x', y') and (x, y) satisfy the following relationship:

$$\begin{pmatrix} x' \\ y' \end{pmatrix} = \begin{pmatrix} \cos\theta & -\sin\theta \\ \sin\theta & \cos\theta \end{pmatrix} \begin{pmatrix} x \\ y \end{pmatrix}. \quad (4)$$

By adjusting the sublattice amplitudes, twist angles, or lattice constants, one can obtain moiré lattice external potentials with different structures. These structures may be periodic or aperiodic, with periodicity primarily determined by the lattice constants and twist angles. Since the lattice constant is typically determined by the wavelength, this study mainly considers the influence of the twist angle on the periodic moiré lattice potential. Therefore, the sublattice amplitudes are fixed at $p_1 = 1, p_2 = 0.5$, and the lattice constant is set to $k = 2$.

Figures 1(a)—(d) illustrate the structures of periodic moiré lattice external potentials for twist angles of $\tan\theta = 7/24, 5/12, 8/15, 3/4$, respectively, where the red boxes indicate a single periodic unit cell. It is evident that the lattice with the smallest twist angle (Figure 1(a), $\tan\theta = 7/24$) exhibits the largest period and the most complex structure, containing potential wells of six different depths within one unit cell. In contrast, the lattice with the largest twist angle (Figure 1(d), $\tan\theta = 3/4$) has the smallest period and the simplest structure, with only two potential well depths in a unit cell. However, we note that the twist angle in Figure 1(c) ($\tan\theta = 8/15$) is slightly larger than that in Figure 1(b) ($\tan\theta = 5/12$), yet its period is slightly larger than the latter. This observation does not fully align with the conclusion that a smaller moiré lattice twist angle corresponds to a larger period[17,18,23,24].

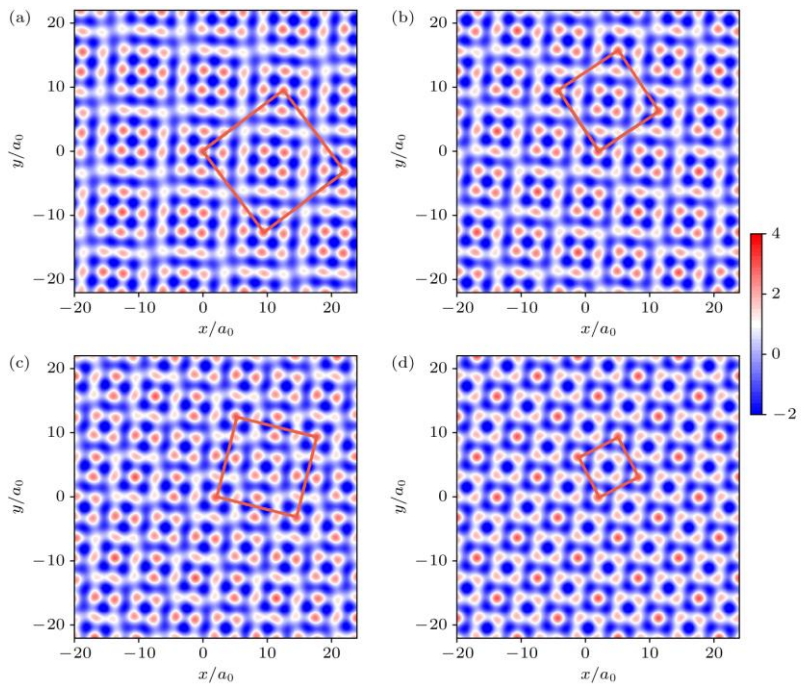

Fig. 1 Moiré periodic potentials for different twist angles ($p_1 = 1, p_2 = 0.5, k = 2$): (a) $\tan\theta = 7/24$**; (b)** $\tan\theta = 5/12$**; (c)** $\tan\theta = 8/15$**; (d)** $\tan\theta = 3/4$**.**

3 Numerical Results Analysis and Discussion

3.1 Band Structure

Seeking the stationary solutions of Equation (2)

$$\Psi(\boldsymbol{r}, t) = \psi(\boldsymbol{r})\mathrm{e}^{-\mathrm{i}\mu t}, \tag{5}$$

Here, μ denotes the chemical potential, and $\psi(\boldsymbol{r})$ satisfies

$$\mu\psi = -\frac{1}{2}\nabla^2\psi + V_{\mathrm{ext}}\psi + g|\psi|^2\psi. \tag{6}$$

If $\psi(\boldsymbol{r})$ is small, the nonlinear term in Equation (6) can be neglected. According to Bloch's theorem, the wave function can then be expressed as

$$\psi(\boldsymbol{r}) = \mathrm{e}^{\mathrm{i}\boldsymbol{k}\cdot\boldsymbol{r}}\phi(\boldsymbol{r}, \boldsymbol{k}), \tag{7}$$

Here, $\phi(\boldsymbol{r}, \boldsymbol{k})$ is a periodic function, and $\boldsymbol{k}$ is the Bloch wave vector. Substituting Equation (7) into Equation (6) yields

$$\mu(\boldsymbol{k})\phi(\boldsymbol{r}, \boldsymbol{k}) = -\frac{1}{2}(\nabla + \mathrm{i}\boldsymbol{k})^2\phi(\boldsymbol{r}, \boldsymbol{k}) + V_{\mathrm{ext}}\phi(\boldsymbol{r}, \boldsymbol{k}). \tag{8}$$

The eigenvalues $\mu(\boldsymbol{k})$ in the eigenvalue problem (8) constitute the Bloch bands. The

band gap located below the lowest band is termed the semi-infinite gap, while the gap between the second and first bands is designated as the first gap, and so forth. Generally, obtaining exact analytical solutions for Equation (8) is challenging; thus, numerical methods such as the finite difference method or the Fourier collocation method are employed[50]. Figure 2 illustrates the Bloch band structures under Moiré periodic potentials with different twist angles. It is evident that the band structures vary significantly with the twist angle. Specifically, smaller twist angles result in flatter low-energy bands.

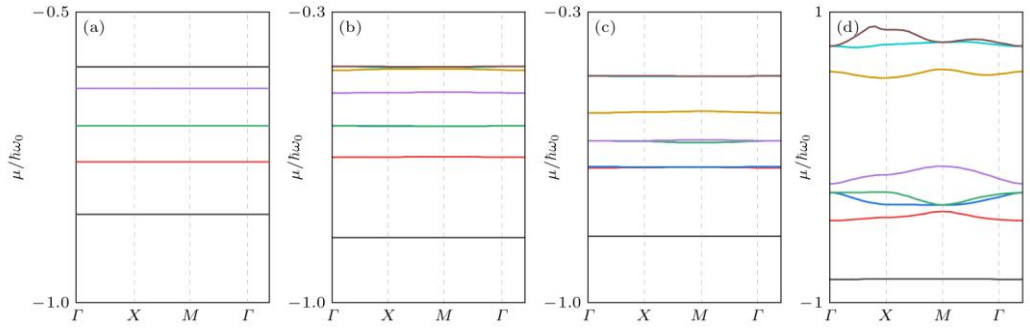

Fig. 2 Band gap structures under periodic moiré potential formed by different twist angles ($p_1 = 1, p_2 = 0.5, k = 2$): (a) $\tan\theta = 7/24$**; (b)** $\tan\theta = 5/12$**; (c)** $\tan\theta = 8/15$**; (d)** $\tan\theta = 3/4$**.**

3.2 Gap Solitons

We employ the Newton-Conjugate Gradient (NCG) method[51] to find soliton solutions to Equation (6), using a Gaussian wave packet as the initial iteration value.

$$\psi(x,y) = \sum_{i=1}^{\mathcal{N}} A_i \exp\left[-\frac{(x-x_i)^2}{W_{x_i}} - \frac{(y-y_i)^2}{W_{y_i}}\right], \tag{9}$$

Here, $\mathcal{N}$ denotes the total number of wave packets; A_i, W_i, and (x_i, y_i) represent the amplitude, width, and central position of the i-th wave packet, respectively. By adjusting these parameters, one can identify gap solitons. Generally, varying the initial iteration values yields gap solitons with diverse structures. However, improper selection may cause the iteration process to diverge or converge to a zero solution. For clarity, we refer to the four Moiré external potentials with angles ($\tan\theta = 7/24, 5/12, 8/15, 3/4$) as External Potentials 1, 2, 3, and 4, respectively.

Using the NCG method, we identified both single-peak and multi-humped solitons in all four potential wells. More complex lattice structures yielded a greater variety of soliton types. To determine whether multi-humped solitons are simple superpositions of single-peak solitons, we analyze the single-peak and double-peak solitons found in External Potential 3, as shown in Figure 3. The results indicate that when the two peaks are widely separated, the density of the double-peak soliton (Figure 3(b)) matches that

of the single-peak soliton (Figure 3(a)). When the peaks are close together, the density of the in-phase double-peak soliton (Figure 3(c)) is slightly lower than that of the widely separated double-peak soliton. In contrast, the out-of-phase double-peak soliton (Figure 3(d)) exhibits a slightly higher density than the widely separated counterpart and displays distinct trailing features. To further compare these four types of solitons, we define

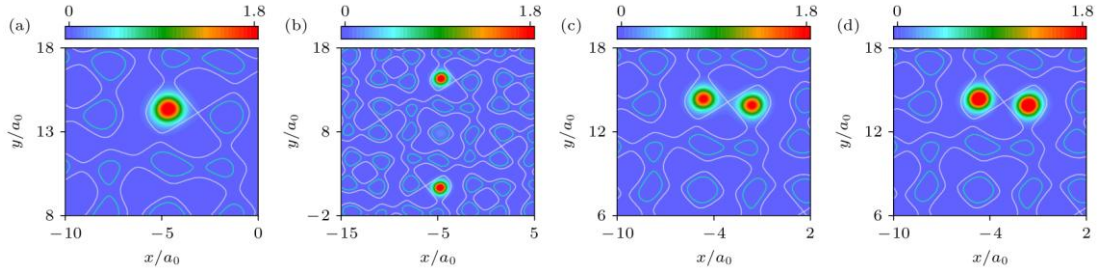

Fig. 3 Single-humped soliton and double-humped solitons: (a) Single-humped soliton; (b) widely separated double-humped soliton; (c) closely separated double-humped in-phase soliton; (d) closely separated double-humped out-of-phase soliton.

$$\begin{aligned} A = max(|\psi|), P = \int |\psi|^2 \mathrm{d}\boldsymbol{r}, \\ E_{\mathrm{kin}} = \frac{1}{2}\int |\nabla\psi|^2 \mathrm{d}\boldsymbol{r}, E_{\mathrm{pot}} = \int V_{\mathrm{ext}}|\psi|^2 \mathrm{d}\boldsymbol{r}, \\ E_{\mathrm{int}} = \frac{1}{2}\int g|\psi|^4 \mathrm{d}\boldsymbol{r}, E_{\mathrm{total}} = E_{\mathrm{kin}} + E_{\mathrm{pot}} + E_{\mathrm{int}}, \end{aligned} \tag{10}$$

Here, A denotes the amplitude, and P represents the particle number. The terms E_{kin}, E_{pot}, E_{int}, and E_{total} correspond to the kinetic energy, potential energy, interaction energy, and total energy, respectively. Figure 4 illustrates the variation of these four soliton types within the semi-infinite gap ($g = -0.1$) as a function of the chemical potential. The four soliton categories exhibit generally consistent trends across the six parameters. Specifically, the amplitude, particle number, and absolute energy values decrease as the chemical potential approaches the first energy band. Since the solitons reside in potential wells with attractive interactions, their kinetic energy is positive, whereas their potential and interaction energies are negative. For well-separated double-peak solitons, the amplitude equals that of single-peak solitons. However, their particle number, kinetic energy, potential energy, and interaction energy are twice those of single-peak solitons. The amplitude, particle number, and absolute energy values of closely spaced in-phase double-peak solitons are slightly lower than those of well-separated double-peak solitons. In contrast, these values for closely spaced out-of-phase double-peak solitons are slightly higher than those of their well-separated counterparts. This indicates that multi-humped solitons are not simple superpositions of single-peak solitons; rather, they constitute distinct structural soliton states.

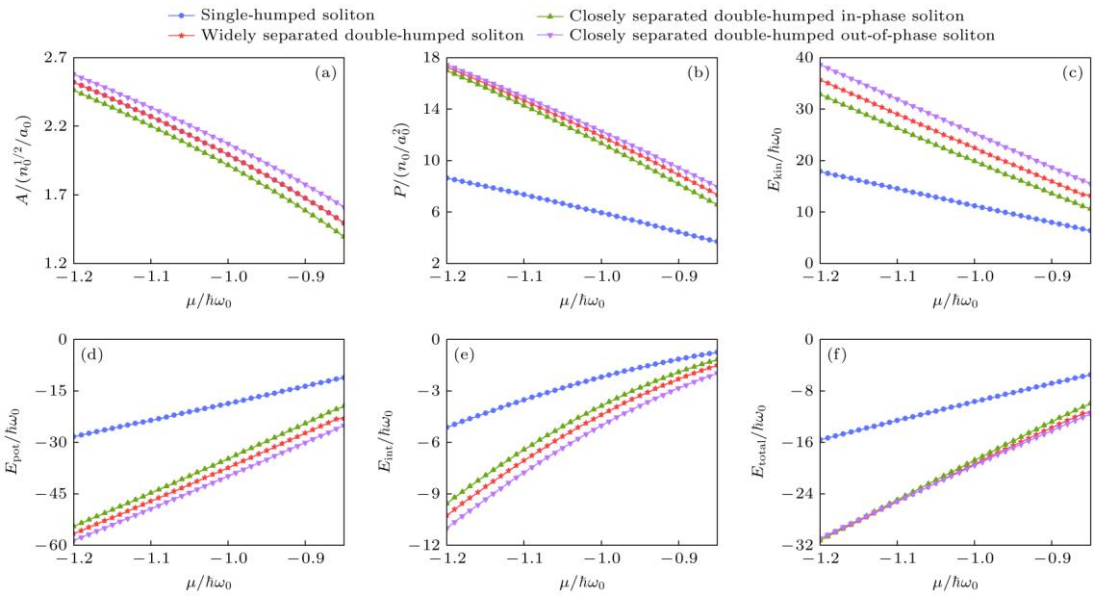

Fig. 4 Variations in the amplitude, particle number, and energy of the four solitons shown in Fig. 3 as functions of the chemical potential: (a) Amplitude; (b) particle number; (c) kinetic energy; (d) potential energy; (e) interaction energy; (f) total energy.

Gap solitons exhibit distinct characteristics in the semi-infinite gap and the first gap. Figures 5(a)—(d) illustrate a type of multi-humped soliton found within one unit cell of the semi-infinite gap for four types of external potentials, with contact interaction $g = -0.1$. It is observed that soliton density remains identical at the same potential well depth. Specifically, deeper potential wells correspond to lower soliton densities, whereas shallower wells correspond to higher densities. This indicates that under attractive contact interactions, particles distribute more extensively in regions with shallower potential wells. However, no solitons were found when the contact interaction g was positive. In the first gap, the contact interaction is set to $g = 1$. Numerical analysis reveals that external potential 4 yields single-peak solitons only in the deepest potential well. External potentials 1, 2, and 3 support solitons in both the deepest and second-deepest wells. However, no solitons were identified in shallower well regions for any of the four external potentials. Figures 6(a)—(d) display a type of soliton state found within one unit cell of the first gap for the four external potentials. It is evident that soliton densities are equal at the same potential well depth. Deeper potential wells correspond to higher soliton densities, while shallower wells correspond to lower densities. This distribution is opposite to that in the semi-infinite gap. It suggests that under repulsive contact interactions, particles preferentially occupy regions with deeper potential wells. Consequently, locating solitons in shallower potential well regions becomes more difficult. Furthermore, we analyzed the influence of contact interaction strength on solitons. We found that in both the semi-infinite gap and the first gap, the soliton amplitude and particle number decrease

as $|g|$ increases. This finding aligns with the conclusions reported in Reference [52].

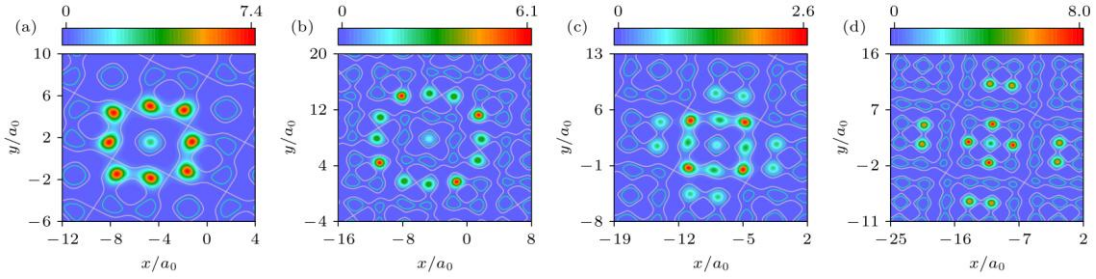

Fig. 5 Solitons in BEC under four moiré periodic potentials in the semi-infinite gap: (a) $\tan\theta = 3/4$**; (b)** $\tan\theta = 8/15$**; (c)** $\tan\theta = 5/12$**; (d)** $\tan\theta = 7/24$**.**

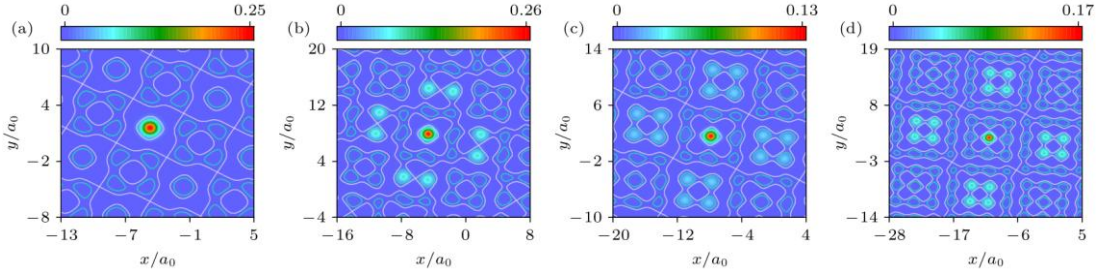

Fig. 6 Solitons in BEC under four moiré periodic potentials in the first gap: (a) $\tan\theta = 3/4$**; (b)** $\tan\theta = 8/15$**; (c)** $\tan\theta = 5/12$**; (d)** $\tan\theta = 7/24$**.**

4 Stability Analysis

Stability constitutes a critical metric for evaluating solitons. Researchers can analyze nonlinear dynamics or linear stability by directly simulating the Gross-Pitaevskii equation (GPE) or employing linearized equations. To assess the linear stability of solitons, we apply the Bogoliubov expansion to the wave function:

$$\begin{aligned}\psi(\boldsymbol{r},t) = \quad & \{\varphi(\boldsymbol{r}) + [v(\boldsymbol{r}) + w(\boldsymbol{r})]\mathrm{e}^{\lambda t} \\ & + [v^*(\boldsymbol{r}) - w^*(\boldsymbol{r})]\mathrm{e}^{\lambda^* t}\}\mathrm{e}^{-\mathrm{i}\mu t},\end{aligned} \tag{11}$$

Here, $|v|, |w| \ll 1$ represent the magnitudes of infinitesimal perturbations, and λ denotes the eigenvalue. If $\mathrm{Re}(\lambda) > 0$, the perturbation amplitude grows exponentially, leading to dynamic instability. Substituting Eq. (11) into Eq. (2) yields the eigenvalue equation

$$L\begin{bmatrix} v \\ w \end{bmatrix} = -\mathrm{i}\lambda\begin{bmatrix} v \\ w \end{bmatrix}, \tag{12}$$

where

$$L = \begin{bmatrix} 0 & -\frac{1}{2}\nabla^2 - \mu + V + g\varphi^2 \\ -\frac{1}{2}\nabla^2 - \mu + V + 3g\varphi^2 & 0 \end{bmatrix}.$$

Equation (12) can be solved using the finite difference method or the Fourier collocation method[50].

Figure 7 presents the linear stability results for solitons within the semi-infinite bandgap. As shown in Figure 7(a), the curves of $\mathrm{Re}(\lambda)$ versus chemical potential μ largely overlap for single-peak solitons, widely separated two-peak solitons, and closely spaced two-peak out-of-phase solitons. These values decrease as μ increases. Within the plotted range, $\sim 10^{-2}$ remains very small ($g = -0.1, \mu = -1$), indicating that these solitons are linearly stable. In contrast, closely spaced two-peak in-phase solitons exhibit $\mathrm{Re}(\lambda)$ values significantly greater than 0 in regions away from the band edge, indicating linear instability. When μ increases to -0.7, the closely spaced two-peak in-phase soliton transitions from linearly unstable to linearly stable. This suggests that soliton stability improves as the chemical potential approaches the band edge. Figures 7(b) and 7(c) display the linear stability spectrum of the single-peak soliton and the linear instability spectrum of the closely spaced two-peak in-phase soliton at $g = -0.1, \mu = -1$. In the first bandgap, extensive numerical calculations show that $\mathrm{Re}(\lambda)$ values for all four types of solitons are very small ($\sim 10^{-2}$), confirming their linear stability.

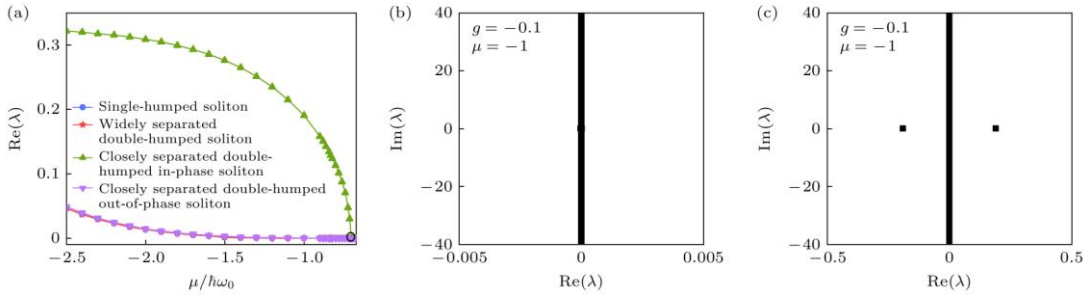

Fig. 7 Linear spectrum of gap solitons in the semi-infinite gap: (a) $\mathrm{Re}(\lambda)$ versus μ for four types of solitons; (b) the single-humped soliton; (c) the closely spaced double-humped in-phase soliton.

To further verify soliton stability, we performed nonlinear dynamic evolution simulations on four types of solitons. At the initial moment, we applied a small perturbation consisting of 1% Gaussian noise to the gap solitons. After prolonged nonlinear evolution, if the soliton amplitude exhibits minimal variation and the waveform remains stable, we classify it as a stable soliton. Conversely, if the soliton shows significant amplitude changes or severe waveform distortion, we determine it to

be dynamically unstable. To characterize soliton stability, we introduce the following ratio:

$$\Delta(t) = \frac{|A(t)-A(0)|}{A(0)}, \tag{13}$$

$\Delta(t)$ denotes the degree of amplitude variation of solitons during dynamic evolution. When $\Delta(t)$ remains small, the soliton amplitude is stable, indicating a steady state. Conversely, if $\Delta(t)$ grows beyond the magnitude of the initial perturbation, the soliton deviates from its initial state and becomes unstable.

We first verify the stability of solitons within the semi-infinite bandgap. We fix the parameters at $g = -0.1, \mu = -1$. The results are shown in Figure 8. The first column displays the initial state of the soliton ($t = 0$). The second column shows the state after long-term evolution ($t = 60$). The third column presents the amplitude variation curve during evolution. The fourth column depicts the linear stability spectrum of the corresponding soliton. Figures 8(a)–(d) illustrate the case of single-peak solitons. The soliton density distribution remains largely unchanged after long-term evolution. Furthermore, $\Delta(t)$ remains minimal, indicating dynamic stability. Figures 8(e)–(h) display two-peak solitons with large peak spacing. The interaction between these solitons is weak due to their significant separation. Thus, they can be treated as two independent single-peak solitons. Their stability aligns with that of single-peak solitons. For two-peak solitons with close peak spacing, the in-phase case (Figures 8(i)–(l)) shows significant changes in soliton density around $t = 25$ under attractive contact interactions. The value of $\Delta(t)$ increases markedly, indicating dynamic instability. In contrast, the out-of-phase two-peak solitons (Figures 8(m)–(p)) exhibit minimal changes in waveform and amplitude. This suggests a minor influence from attractive contact interactions, and the solitons remain dynamically stable. The stability characteristics of other multi-humped soliton types are consistent with those of two-peak solitons.

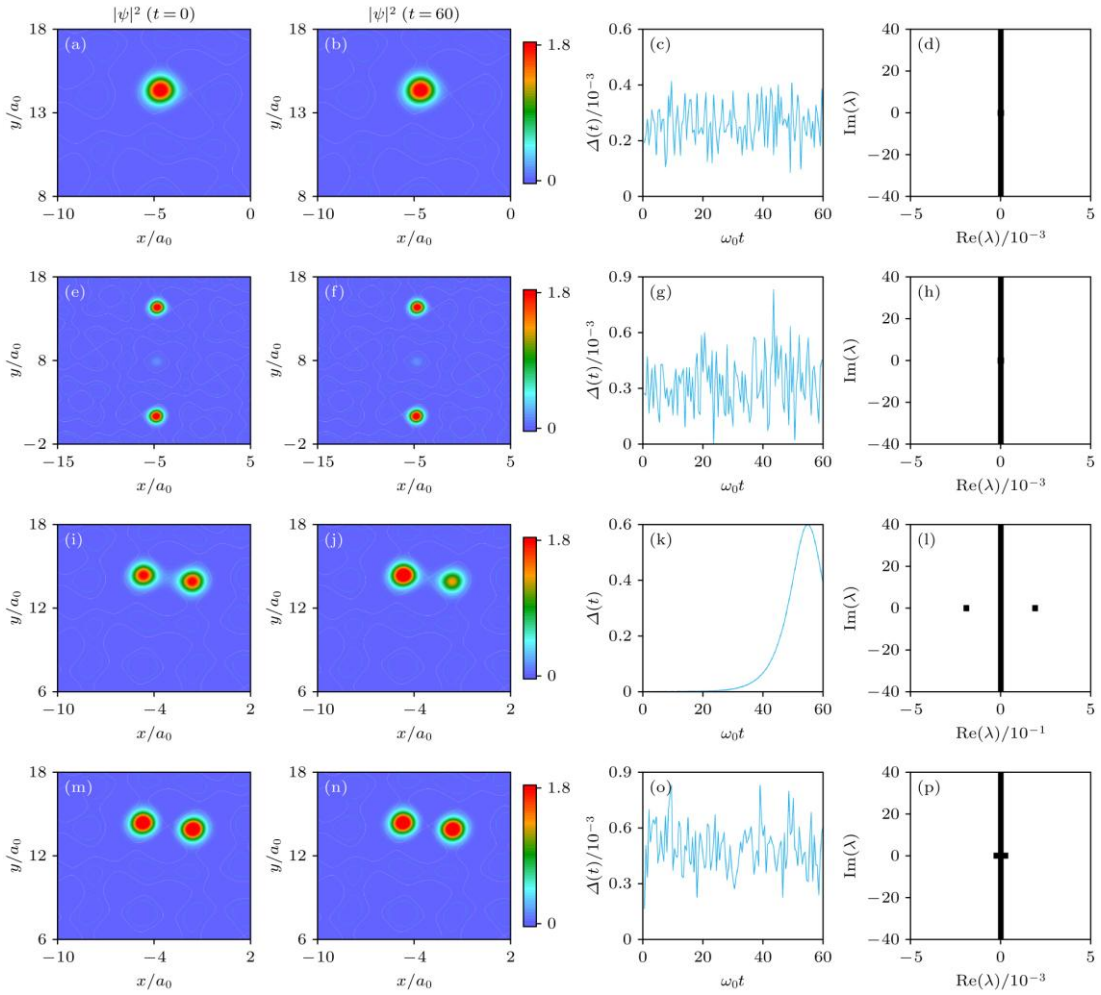

Fig. 8 Nonlinear dynamical stability of solitons in the semi-infinite gap during time evolution: (a)-(d) single-humped soliton; (e)-(h) widely separated double-humped soliton; (i)-(l) closely separated double-humped in-phase soliton; (m)-(p) closely separated double-humped out-of-phase soliton.

Figure 9 illustrates the nonlinear dynamic evolution of solitons within the first gap, with parameters set to $g = 1, \mu = -0.6$. The single-peak soliton (Figures 9(a)-(d)) remains stable. Multi-humped solitons with widely separated peaks exhibit properties similar to those of single-peak solitons and are also dynamically stable. For closely spaced in-phase two-peak solitons (Figures 9(e)-(h)) and out-of-phase two-peak solitons (Figures 9(i)-(l)), stability persists despite the short inter-peak distance. This stability arises because the repulsive interatomic contact interaction enhances soliton localization under lattice confinement. The stability characteristics of other closely spaced multi-humped solitons align closely with those of two-peak solitons. These findings indicate that the results of nonlinear dynamic evolution are consistent with those of linear stability analysis.

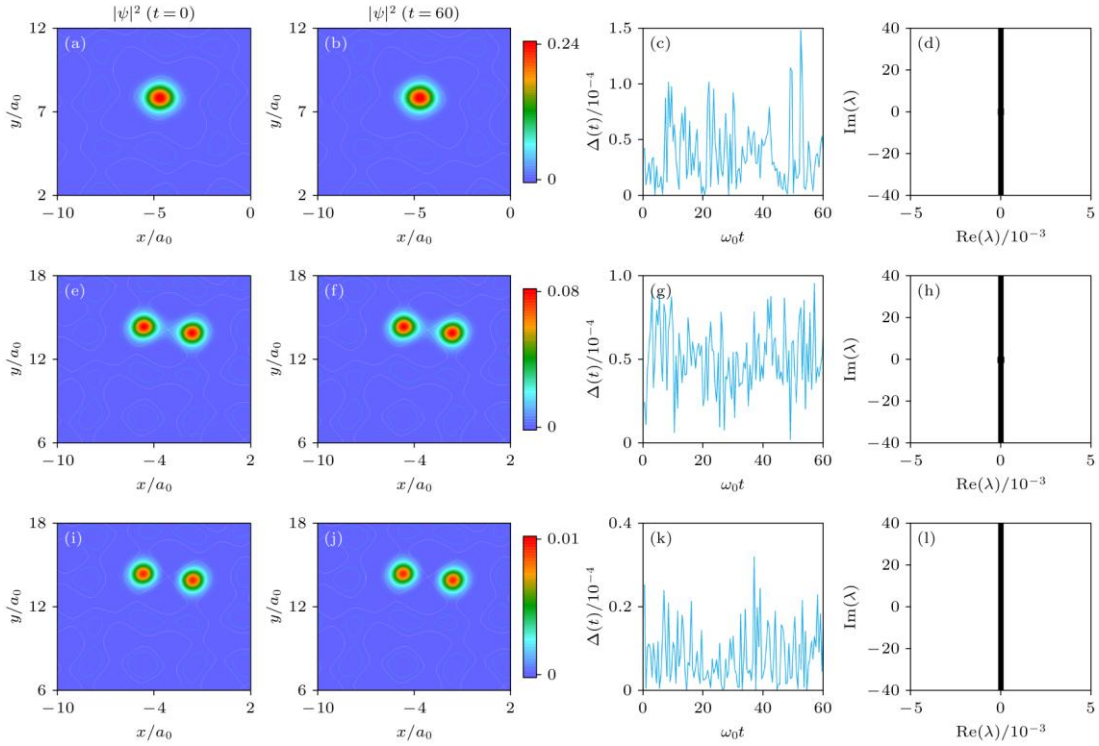

Fig. 9 Nonlinear dynamical stability of solitons in the first gap during time evolution: (a)-(d) single-humped soliton; (e)-(h) closely spaced double-humped in-phase soliton; (i)-(l) closely spaced double-humped out-of-phase soliton.

5 Conclusions and Outlook

This study investigates gap solitons and their stability in Bose-Einstein condensates (BECs) within moiré periodic potentials featuring various twist angles. The results reveal that the twist angle significantly modulates the moiré period length and the flatness of low-energy bands. When the difference between twist angles is large, smaller twist angles generally correspond to larger moiré periods and flatter low-energy bands. However, this trend does not fully hold when the difference in twist angles is small. Furthermore, smaller twist angles lead to more complex lattice external potential structures. This complexity alters the position and width of band gaps, thereby influencing the properties of gap solitons. Using the Newton-conjugate gradient method, we identified various types of solitons in moiré lattice potentials with four different twist angles. We observed that smaller twist angles allow solitons to exist across a wider range of potential well depths. The density distributions of solitons exhibit distinct behaviors in different band gaps. In the semi-infinite gap, attractive interactions dominate; consequently, deeper potential wells result in smaller soliton density distributions. In contrast, repulsive interactions dominate in the first gap, where deeper potential wells lead to larger soliton density distributions. Linear stability analysis and nonlinear dynamic evolution demonstrate that solitons found in the first

gap, including both single-peak and multi-peak structures, exhibit robust dynamic stability. However, in the semi-infinite gap, single-peak solitons show good stability, whereas multi-humped solitons with small peak spacing exhibit weaker stability. Stability improves as solitons approach the band edge. These findings not only deepen the understanding of nonlinear localized states in moiré superlattices but also provide theoretical guidance for future experiments on manipulating BEC solitons in moiré lattices via twist angle engineering.

References

[1] Chen W, Mills D L 1987 *Phys. Rev. Lett.* **58** 160

[2] Sipe J E, Winful H G 1988 *Opt. Lett.* **13** 132

[3] Mills D L, Trullinger S E 1987 *Phys. Rev. B* **36** 947

[4] Sakaguchi H, Malomed B A 2006 *Phys. Rev. E* **74** 026601

[5] Baizakov B B, Malomed B A, Salerno M 2003 *Europhys. Lett.* **63** 642

[6] Bloch I, Dalibard J, Nascimbene S 2012 *Nat. Phys.* **8** 267

[7] Rodas-Verde M I, Michinel H, Pérez-García V M 2005 *Phys. Rev. Lett.* **95** 153903

[8] Ngo T V, Tsarev D V, Lee R K, Alodjants A P 2021 *Sci. Rep.* **11** 19363

[9] Fleischer J W, Segev M, Efremidis N K, Christodoulides D N 2003 *Nature* **422** 147

[10] Louis P J, Ostrovskaya E A, Peng P, Savage C M, Kivshar Y S 2003 *Phys. Rev. A* **67** 013602

[11] Ostrovskaya E A, Kivshar Y S 2003 *Phys. Rev. Lett.* **90** 160407

[12] Chen Z P, Malomed B A 2017 *Phys. Rev. E* **95** 032217

[13] Sakaguchi H, Malomed B A 2018 *Phys. Rev. A* **97** 013607

[14] Fu Q D, Wang P, Huang C, Kartashov Y V, Torner L, Konotop V V, Ye F W 2020 *Nat. Photonics* **14** 663

[15] Wang P, Fu Q D, Li Y R, Ye F W 2021 *Chin. Opt.* **14** 986

[16] Wang P, Zheng Y L, Chen X F, Huang C M, Kartashov Y V, Torner L, Konotop V V, Ye F W 2020 *Nature* **577** 42

[17] Cao Y, Fatemi V, Demir A, Fang S, Tomarken S L, Luo J Y, Sanchez-Yamagishi J D, Watanabe K, Taniguchi T, Kaxiras E, Ashoori R C 2018 *Nature* **556** 80

[18] Cao Y, Fatemi V, Fang S, Watanabe K, Taniguchi T, Kaxiras E, Jarillo-Herrero P 2018 *Nature* **556** 43

[19] Yankowitz M, Chen S, Polshyn H, Zhang Y, Watanabe K, Taniguchi T, Graf D, Young A F, Dean C R 2019 *Science* **363** 1059

[20] Lu X B, Stepanov P, Yang W, Xie M, Aamir M A, Das I, Urgell C, Watanabe K,

Taniguchi T, Zhang G, Bachtold A 2019 *Nature* **574** 653

[21] Yuan L, Zheng B Y, Kunstmann J, Brumme T, Kuc A B, Ma C, Deng S B, Blach D, Pan A L, Huang L B 2020 *Nat. Mater.* **19** 617

[22] Wang J, Mu X, Wang L, Sun M 2019 *Mater. Today Phys.* **9** 100099

[23] Andrei E Y, MacDonald A H 2020 *Nat. Mater* **19** 1265

[24] Kennes D M, Claassen M, Xian L, Georges A, Millis A J, Hone J, Dean C R, Basov D N, Pasupathy A N, Rubio A 2021 *Nat. Phys.* **17** 155

[25] Carr S, Massatt D, Fang S, Cazeaux P, Luskin M, Kaxiras E 2017 *Phys. Rev. B* **95** 075420

[26] Deng Y, Oudich M, Gerard N J, Ji J, Lu M 2020 *Phys. Rev. B* **102** 180304

[27] Eiermann B, Anker T, Albiez M, Taglieber M, Treutlein P, Marzlin K P, Oberthaler M K 2004 *Phys. Rev. Lett.* **92** 230401

[28] Lobanov V E, Kartashov Y V, Konotop V V 2014 *Phys. Rev. Lett.* **112** 180403

[29] Kartashov Y V, Konotop V V, Abdullaev F K 2013 *Phys. Rev. Lett.* **111** 060402

[30] Zhang Y P, Xu Y, Busch T 2015 *Phys. Rev. A* **91** 043629

[31] Su J, Lyu H, Chen Y Y, 2021 *Phys. Rev. A* **104** 043315

[32] Morsch O, Oberthaler M 2006 *Rev. Mod. Phys.* **78** 179

[33] Meng H J, Wang J, Fan X B, Wang Q Q, Shao K H, Zhao Y X, Wang W Y, Shi Y R 2022 *Phys. A* **598** 127337

[34] Meng H J, Wang J, Fan X B, Wang Q Q, Shao K H, Zhao Y X, Wang W Y, Shi Y R 2023 *Phys. Rev. E* **108** 034215

[35] O'Riordan L J, White A C, Busch Th 2016 *Phys. Rev. A* **93** 023609

[36] González-Tudela A, Cirac J I 2019 *Phys. Rev. A* **100** 053604

[37] Lian B, Wang Z J, Bernevig B A 2019 *Phys. Rev. Lett.* **122** 257002

[38] Meng Z M, Wang L W, Han W, Liu F D, Wen K, Gao C, Wang P J, Chin C, Zhang J 2023 *Nature* **615** 231

[39] Gómez-Urrea H A, Ospina-Medina M C, Correa-Abad J D, Mora-Ramos M E, Caro-Lopera F J 2020 *Opt. Commun.* **459** 125081

[40] Zhang Z, Wang Y, Watanabe K, Taniguchi T, Ueno K, Tutuc E, LeRoy B J 2020 *Nat. Phys.* **16** 1093

[41] Utama M I, Koch R J, Lee K, Leconte N, Li H, Zhao S, Jiang L, Zhu J, Watanabe K, Taniguchi T, Ashby P D 2021 *Nat. Phys.* **17** 184

[42] Balents L, Dean C R, Efetov D K, Young A F 2020 *Nat. Phys.* **16** 725

[43] López M R, Peñaranda F, Christensen J, San-Jose P 2020 *Phys. Rev. Lett.* **125** 214301

[44] Tu P, Wang Q Q, Ma J P, Shao K H, Zhao X, Xi B L, Zhang X F, Shi Y R 2025

Chaos Solitons Fractals **190** 115773

[45] Tu P, Ma J P, Zhao X, Xi B L, Shao K H, Zhang X F, Shi Y R 2025 *Phys. A* **666** 130504

[46] Xu L, Chen S L, Yang X Y, Zhang X F 2023 *Acta Phys. Sin.* **72** 100307

[47] Petrov D S, Holzmann M, Shlyapnikov G V 2000 *Phys. Rev. Lett.* **84** 2551

[48] Hadzibabi Z, Krüger P, Cheneau M, Battelier B, Dalibard J 2006 *Nature* **441** 1118

[49] Shi Y R, Wang X L, Wang G H, Liu C B, Yang H J 2013 *Commun. Theor. Phys.* **59** 273

[50] Yang J K 2010 *Nonlinear Waves in Integrable and Nonintegrable Systems*（Philadelphia: SIAM） p269

[51] Yang J K 2009 *J. Comp. Phys.* **228** 7007

[52] Meng H J, Zhou Y S, Li X L, Wan X H, Zhou Z K, Wang W Y, Shi Y R 2021 *Physica A* **577** 126087